Numerical Flow Simulations past a Bell 412 Helicopter in Real-Time Hover, Low and High Forward Speed Flight Conditions Using Chimera Grid Technique

F. Zhang, H. Xu, N. G. Ball and A.W. Gubbels

Institute for Aerospace Research (IAR)
National Research Council of Canada (NRC)
Ottawa, Ontario, Canada, K1A 0R6
(Tel: +1-613-998-3410; E-mail: Steve.Zhang@nrc.ca)

Abstract: The current research investigates the unsteady flow past the Bell 412 helicopter (fuselage and main rotor) in hover and forward flight conditions with rotor blades moving in real-time including collective and cyclic blade pitch motions using a Chimera structured moving grid method. The background grid is around the fuselage, and the child grid is around each blade of the main rotor. The calibrated relation relating control positions to the blade pitch angle was input to CFD-FASTRAN flow solver to simulate the blade motion. The calibration was verified by the comparison of computational total lift against the measured helicopter weight in hover. The pressure distributions around the rotor blades were reasonable and periodically changed with the blade pitching motion and the rotor rotation. The pressure measurements on the fuselage qualitatively agreed with the computational results at discrete locations. The unidirectional rotation of the rotor leads to flow asymmetry on the fuselage for hover and low forward flight conditions. As forward speed increases, the impact of the rotor rotation on the fuselage pressure results is reduced.

Keywords: Bell 412 helicopter, Unsteady flows, Computational Fluid Dynamic (CFD) Simulation, Hover, Forward flight, Chimera moving grid method.

1. INTRODUCTION

The flow past a helicopter such as the Bell 412 is very complex and unsteady. Rotation of the rotor, flapping and pitching of the blades, and their subsequent interaction with the fuselage have a significant effect upon the overall performance of the helicopter. During hover, the rotor blades move large volumes of air in a downward direction, which alters the relative wind and changes the angle of attack of the blades. Also, the downwash of the preceding blade severely affects the lift of the following blades. These situations require an increase of the collective pitch of the rotor blades to produce enough aerodynamic force to sustain a hover. The efficiency of the hovering rotor system is improved in the low speed forward flight condition of approximately 10 – 20 knots. As the incoming wind enters the rotor system, turbulence and vortices are left behind and the flow of air becomes more horizontal and the impact of the rotor on the fuselage is focused on the rear part of the fuselage. At the same time, the tail rotor becomes more aerodynamically efficient because it works in progressively less turbulent air as flight speed increases. The lift increase related to this improvement is called translational lift. At high forward speeds, the air passing through the rotor system is nearly horizontal and the impact of the rotor system on the fuselage is greatly reduced. The pressure distributions on the fuselage are almost symmetric in both port and starboard sides. However, in high speed forward flight, the retreating blade stall becomes a major problem. As forward speed increases, the airspeed over the retreating blade (the blade moving away from the direction of flight) slows down. The angle of attack (pitch angle) of the blade must be increased to produce an amount of lift equal to that of the advancing blade (the blade moving in the direction of flight). As this angle increase is continued, the retreating blade will stall at some certain high forward speed. Just as the stall of an airplane wing limits the low speed of the airplane, the stall of a retreating blade of the rotor limits the maximum speed of a helicopter.

The numerical simulation of the flow past a complete helicopter is still very challenging. Considerable work has been done in this area [1 – 7]. However, most of it is focused on CFD studies for isolated rotors or complete helicopters with a simplified fuselage. The available work for a complex helicopter configuration such as the Bell 412 is very limited.

Previously at IAR, the unsteady flow past a simple helicopter configuration known as the Robin under a forward flight condition [8] and the Bell 412 helicopter (fuselage and main rotor) under a hover flight condition (case 1) [9] with rotor blades moving in a real-time collective and cyclic pitching were successfully investigated using Chimera structured moving grid method with the CFD solver CFD-FASTRAN [10]. The agreement between the computation and experimental data was reasonable. Traditionally, the pitch angles for each of the blades of the rotor are considered to be the same for a helicopter in hover. However, in practice (reference 9), two main reasons, non-zero wind and the uneven distribution of mass of the helicopter and installed equipment cause the centre of aerodynamic lift and the centre of the gravity to be not aligned. In order to overcome these effects, and to maintain a steady hover, the blades must pitch individually with azimuth as they do in forward flight. In this study, two more flight-tested flow cases for the Bell 412 helicopter [11] with low (18.86 knots, case 2) and high (81.23 knots,

case 3) forward flight speeds were numerically simulated, respectively. The numerical results were compared with the corresponding measured data on the fuselage. Because the measurement points were very scattered on the surface of fuselage, the pressure data of the computation were extracted out and compared with the measurement at the points only fallen into or close to the corresponding station cuts. With consideration for computer resources, Euler computations were carried out in the present study.

In addition to the complexities of the flow physics modeling, the grid generation for a helicopter fuselage and rotor presents another daunting challenge. This is the most time consuming aspect of a typical CFD simulation. The multi-block structured computational grid used in this study was generated interactively on a Silicon Graphics workstation using ICEMCFD Hexa.

2. GEOMETRY DESCRIPTION AND GRID GENERATION

This CFD study was only carried out for the Bell 412 helicopter configuration with the fuselage and the main rotor with four blades. The tail rotor was not included. The original CAD geometry is from Bell Helicopter Textron. The blade cross-section has non-uniform profiles and is twisted in the span-wise direction, with the blade chord being tapered near the tip (Figure 1). The rotor radius is R=7m and the averaged rotor blade chord length is c=0.37m. The coning angles (from the measurement) used in the simulation were 11.23, 12.28 and 11.31 degrees for these three cases, respectively. The rotational speed of the main rotor is ω=324rpm (33.93rad/s), which gives the tip speed at 237.5m/s (Mach number 0.70).

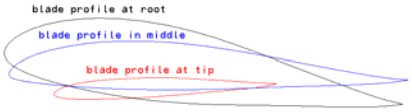

Figure 1. Blade section profiles

The multi-block structured computational grid was generated interactively on a Silicon Graphics workstation using ICEMCFD Hexa, which is a three-dimensional object-based, semi-automatic, multi-block surface and volume mesher. The background grid is around the fuselage. The child grid is around each blade of the rotor, which was generated separately. The flow field around the fuselage is asymmetrical because of the rotation of the rotor. Therefore, the computation for the complete helicopter must be simulated and a grid around the complete fuselage is needed. Previous experience on complex grid topologies has shown that the overall framework and the multi-block structured grid have to be meticulously planned to accommodate such a complex geometry as a Bell 412 helicopter fuselage. There should be as few blocks as possible in the background grid which were involved with the child grids to ensure the chimera grid strategy was carried out smoothly and efficiently. Therefore, two grid blocks large enough to hold the complete rotor grid were formed above the fuselage in the background grid (Figure 2). For the child grids, the mesh around one blade was generated first. Then they were copied and moved to form the meshes for the other blades (Figure 2). At the same time, the coning angle of the rotor and the initial pitch angle for each blade were also considered. It should be noted that the domain of the child grid must be large enough to accommodate the hole cutting (around the blade) and to ensure as few orphan grid points as possible (no orphan points is the best) in carrying out of the chimera grid strategy.

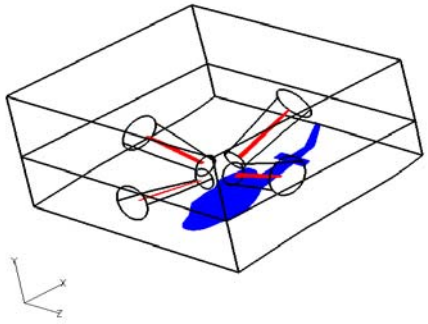

Figure 2. Two blocks in the background holding the child grid domains

Euler computations were carried out because of the limited computer resources. The background grid (around the fuselage) contained 153 blocks, which accommodates the complex and detailed configuration. The total number of grid points was about 1.73 million unevenly distributed within the blocks. One child grid around a blade contained 6 blocks with about 0.1 million nodes. There were 69 mesh points along the profile of the blade in the chord-wise direction and 57 mesh points in the span-wise direction. The grid point distribution in the two large blocks above the fuselage was similar to that in the child grid blocks, which made the flow properties exchange between the parent (background) and child grids correct and smooth.

3. ROTOR BLADE MOTION

The main rotor rotates with respect to the inertial system. The flapping, pitching and lagging of the blades are with respect to the rotation of the rotor.

In flight data collection [11] was performed by the Flight Research Laboratory (FRL) of IAR. The flight measured data included the pressure distributions on the Bell 412 fuselage surface, the flapping and lagging motion of the blades, the collective control position (corresponding to the blade collective control) and the lateral and longitudinal control positions (corresponding to the blade cyclic control). For simplicity, lagging was not included in the current study. Flapping was replaced by its averaged value, coning. Then, the relationship between control positions and rotor-blade pitch angle was determined.

According to the reference 11, as illustrated in Figure 3, for Bell 412 helicopter, the limiting control positions are: (1) longitudinal stick positions at 6.0 inches of forward-stop and -6.0 inches of aft-stop; (2) lateral stick positions at 6.0 inches of starboard-stop and -6.0 inches of port-stop; (3) collective stick positions at 0.0 inches of down-stop and 10.7 inches of up-stop (not shown here). The reference also provided the calibrations between the control positions and the blade pitch angle (Tables 2 and 3 in reference 11) at the five azimuth angles of 103, 148 193, 238 and 283 degrees (0 degrees is the angle when the trailing blade is parallel to the aircraft longitudinal axis). At these azimuth angles, the blade pitch angle θ was linearly linked with the collective control stick position when the longitudinal stick is at either forward-stop or aft-stop position and the lateral stick at either port-stop or starboard-stop position. Similar relations exist between the blade pitch angle and the longitudinal and lateral stick positions, respectively. Based on these relations, a formula was determined to obtain the blade pitch angles at these five azimuth angles for any combination of collective, longitudinal and lateral stick control positions.

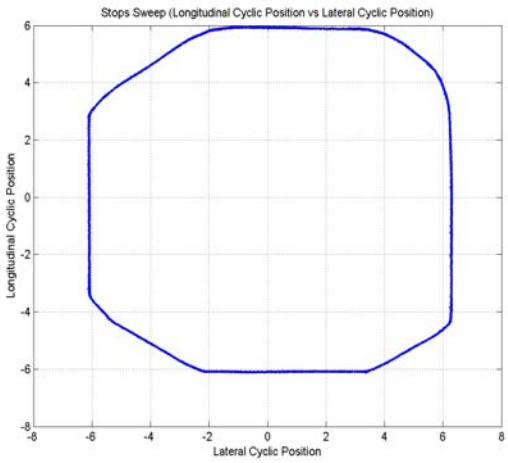

Figure 3. Blade cyclic sweep at the stops

In the hover case and two forward flight cases, the collective, longitudinal and lateral control stick positions were shown in table 1.

	collective	longitudinal	lateral
Case1	4.30	-0.13	2.10
Case2	5.56	-0.30	-0.25
Case3	4.60	0.98	0.85

Table 1. Collective, longitudinal and lateral control stick positions, inches

By using the formula, the corresponding pitch angles at the five azimuth angles were shown in table 2.

azimuth	103	148	193	238	283
Case1	1.28	4.32	8.88	12.96	13.59
Case2	3.44	4.04	7.46	12.22	15.02
Case3	-0.59	1.95	7.63	13.74	16.25

Table 2. Pitch angles at the five azimuth angles, degrees

The curve-fitting method was then applied to the five discrete blade pitch angles for each case, resulting in the blade motion schedules (Figure 4) as follows

$$\theta = \theta_0 - A\sin(\omega t - \varphi_0)(\deg.)$$

	θ_0	A	φ_0
Case1	7.43	6.16	0.0
Case2	9.20	6.0	30.0
Case3	7.82	8.42	15.0

Table 3. Blade motion schedules, degrees

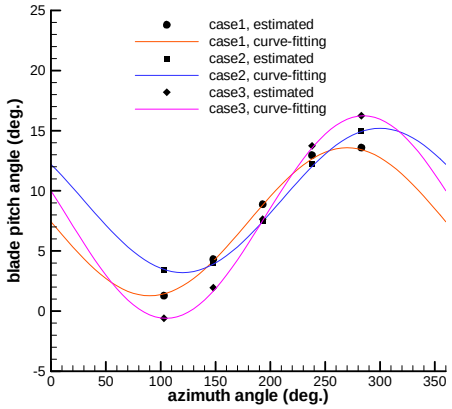

Figure 4. Blade motion schedules

where t is the time in second, ωt the azimuth angle. From these schedules, the starting pitch angles for blade 1, 2, 3 and 4 (The trailing blade is numbered 1. Then other blades are numbered 2, 3 and 4 in counterclockwise direction from the top view of the helicopter) for each case are obtained as shown in table 4.

	Blade 1	Blade 2	Blade 3	Blade 4
Case1	7.43	1.27	7.43	13.59
Case2	12.20	4.00	6.20	14.40
Case3	10.00	-0.31	5.64	15.95

Table 4. Starting pitch angles for each blade, degrees

The information about the rotor rotation, blade motion and initial pitch angles was used as input to the CFD-FASTRAN flow solver to simulate the unsteady flows past Bell 412 helicopter.

4. MATHEMATICAL MODEL AND NUMERICAL ALGORITHM

In this study, the governing equations used are the unsteady form of the Euler equations with a general moving rigid grid [10] which were derived by applying conservations of mass, momentum and energy to a control volume V with a boundary ∂V in a Cartesian coordinate system. The integral form of the governing equations can be written as:

$$\frac{d}{dt}\int_V Q dV + \int_{\partial V} (\vec{F} - Q\vec{v_g}) \bullet \vec{n} ds = \int_V \Omega dV$$

where Q and $\vec{F}$ are the conservative variables and the flux vectors. $\vec{v_g}$ is the moving grid velocity. $\vec{n}$ and s are the outward normal vector and surface area of the control volume, respectively. Ω is the source term.

The child grid domains are moving with the rotation of the rotor and pitching of the blades. The background (parent) grid is not moving, which means $\vec{v_g} = 0$.

On the blade surfaces or fuselage, the flux is zero, which means that $(\vec{v} - \vec{v_g}) \bullet \vec{n} = 0$ and $\vec{v} \bullet \vec{n} = 0$ are applied on them, respectively. Here $\vec{v}$ is the velocity vector. The inlet and exhaust of the engine were also set as solid walls. The overset (Chimera) boundary condition was applied on the outside boundaries of the child domains. The farfield boundary condition was applied on the outside of the background domain.

During the implementing of the Chimera grid technique, a hole is instantaneously created and updated around a blade within the parent grid at each time step. The edge of the hole is called fringe which is included in the child grid. The parent grid (receiver) takes the flow information from the child grid (donor) and the child grid (receiver) takes the flow information from the parent grid (donor) on the fringe. The solutions in both grids are instantaneously updated as the blade is moving. The information exchange between the parent and the child grids is performed by using a tri-linear interpolation technique (non-conservative) with the search for the donor grid cells, which is proceeded at each time step in the truly unsteady computation.

The flux vector and the flux Jacobians are evaluated using Roe's approximate Riemann solver, which is a flux difference scheme. The second-order spatial accuracy is achieved using Minmod gradient limiters. The fully implicit Point Jacobi scheme is selected for the time integration. The sub-iterations are fixed at 40 and the tolerance is 10^{-4}. More detailed information about the numerical algorithm and Chimera technique can be found in the CFD-FASTRAN manual [10].

In this study, the time step intervals were Δt = 0.000061728, 0.00007716 and 0.00005144 seconds for each case, which correspond to an increment of 0.12, 0.15 and 0.10 degrees in the rotor azimuth angle (3000, 2400 and 3600 time steps in a revolution of the rotor, respectively). One time step took about 156 seconds (no parallel computation) to run. Therefore, a complete revolution required about 105, 132 and 87.5 CPU hours for each case in the DART computer at IAR. It was noted that convergence needed more than 6 revolutions. Obviously, the simulation for Navier-Stokes equations would take much more time for the CPU. Thus parallel computing is recommended for the simulation within a reasonable amount of time.

5. RESULTS AND DISCUSSIONS

Flight measured data was reported [11] using dimensional values, and therefore the computational results are presented in the same fashion to allow comparison between them. Table 5 gives the parameters of three flow cases.

	V_∞ (knots)	P (pa)	T (k)	α (deg.)	β (deg.)
Case1	0.0	99989.49	288.18	n/a	n/a
Case2	18.86	99236.59	299.50	-0.22	11.93
Case3	81.23	96802.05	297.29	3.39	-1.39

Table 4. Parameters of flow cases

where V_∞ is the flight speed. P is the static pressure and T is the static temperature. α and β are angles of attack and sideslip.

In helicopter aerodynamics, hover is a critical case. It is usually used to judge the accuracy of numerical investigation. Figure 5 provides a comparison between the total computed lift (time-averaged 45378.8N) and the measured helicopter weight (46136.0N) for hover. Ideally, they should be equal each other. However, the figure shows a 1.6% difference between them. Because the rotor has 4 blades, the lift has 4 periodic changes in a revolution. It is predicted that the other flow parameters have a similar periodical change with the rotation of the rotor. It should be noted that the total lift is the sum of rotor lift (from 4 blades) and the fuselage lift (usually, fuselage lift is negative in the hover as the rotor downwash impinges on the fuselage.). The lift from each individual rotor blade is shown in Figure 6.

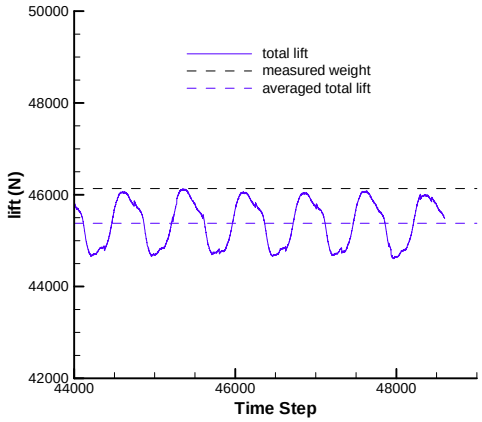

Figure 5. Total lift compared with measured helicopter weight, hover

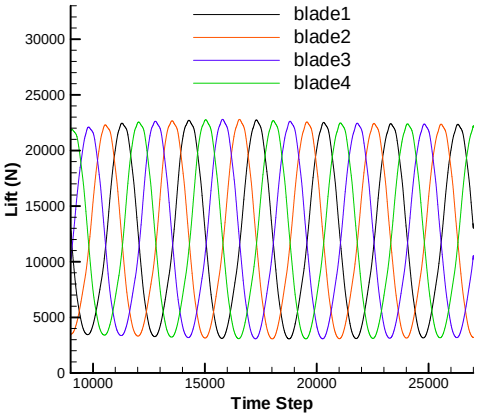

Figure 6. Lift on the blades, hover

Figure 7 displays the streamlines going through the rotor disc for the three flow cases and corresponding velocity vectors. In hover situation, the rotor blades move large volumes of air in a downward direction. The whole fuselage is in this downwash. It is observed that the flow is not central-symmetric as that in traditional hover because the pitch angle of each blade is different from each others in practical hover as mentioned earlier. At the low forward flight condition, the flow of air becomes more horizontal. The downwash of the rotor does not affect the nose part of the fuselage. At the high forward flight condition, the air passing through the rotor system is nearly horizontal. The impact of the rotor system on the fuselage is expected to be greatly reduced.

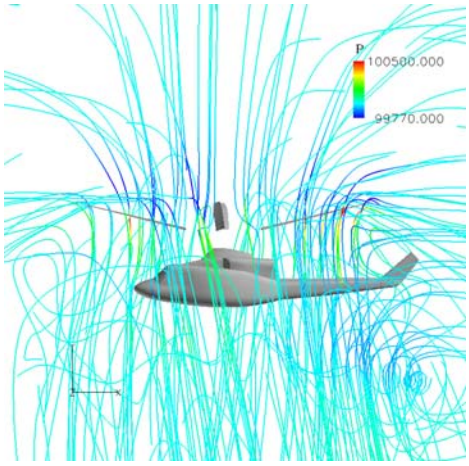

Figure 7a. Streamlines, hover

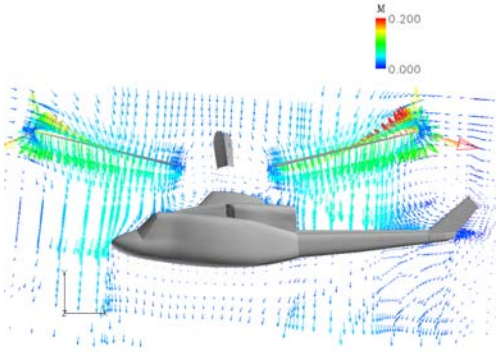

Figure 7b. Velocity vectors, hover

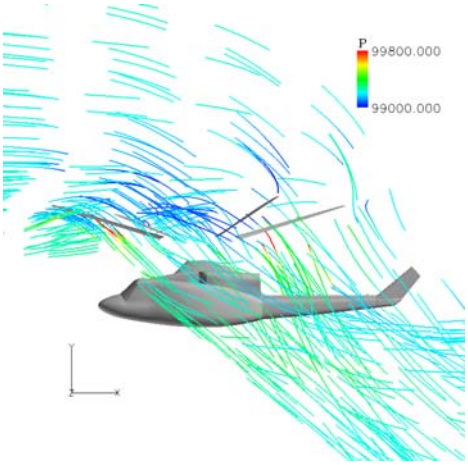

Figure 7c. Streamlines, 18.86 knots

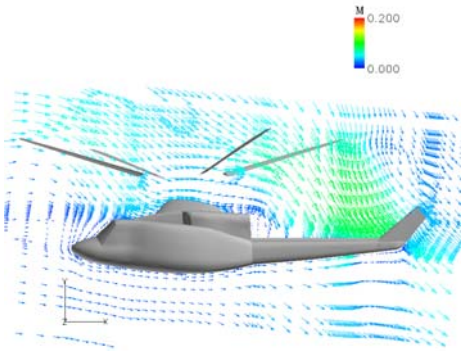

Figure 7d. Velocity vectors, 18.86 knots

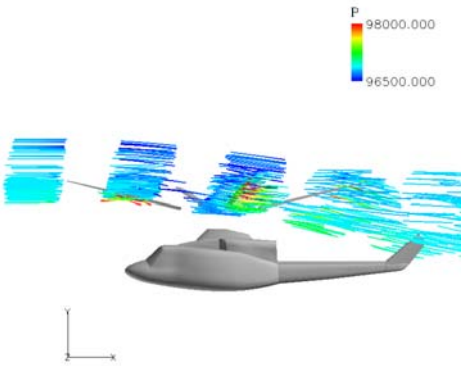

Figure 7e. Streamlines, 81.23 knots

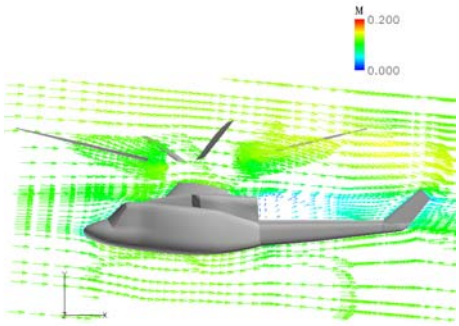

Figure 7f. Velocity vectors, 81.23 knots

Figure 7. Streamlines cross the rotor disc and Velocity vectors on the symmetric plane of the fuselage

Pressure data was not recorded on the blade surfaces in flight. Therefore, only the computational results are shown here. Figure 8 displays the section pressure distributions on the blades at 50% span-wise location. The corresponding pitch angles for each blade are given in Table 5 according to the blade motion schedules in Figure 4. Based on our experience with numerical simulation for the flow past a blade, the results here are reasonable. In the hover condition (Figure 8a), blade 4 provides the maximum load among the four blades because it has the highest pitching angle. Blade 2 gives the minimum load as it experiences lowest pitch angle. On the blades 1 and 3, although their pitch angles are same, their loads are apparently different from each other. This is a specific characteristic of unsteady flows. The reason is that the position of blade 1 is time-historically in the pitching-down phase and that of blade 3 in the pitching-up phase. For forward flight conditions (Figures 8b and 8c), the situation is different. Although blade 4 has the maximum pitch angle, it has not the maximum load because it is the retreating blade. The similar situation happens for the advancing blade 2 with the minimum pitch angle. For other two blades, one is in the pitching-down phase and another in the pitching-up phase. Their loads are different from each other. The retreating blades (port side) have to increase the pitch angle to increase the load and the advancing blades (starboard side) have to reduce the pitch angle to reduce the load, which makes the balance between the port side and the starboard side. Figure 9 displays the pressure contours on a blade upper surface at the various azimuth angles for the three flow cases. It is clear that the distributions are different at the different azimuth angles even for the hover condition.

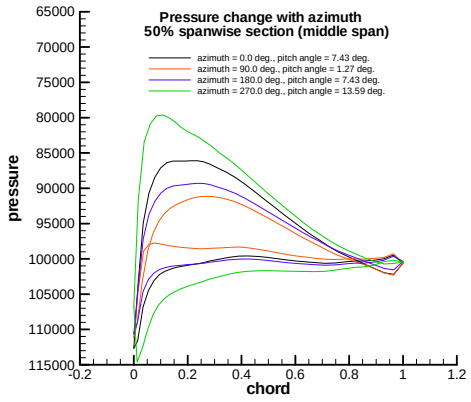

Figure 8a. Hover

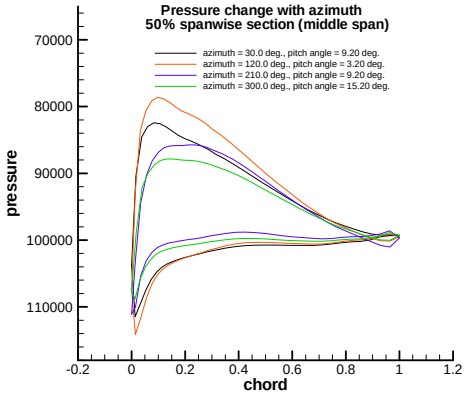

Figure 8b. Forward, 18.86 knots

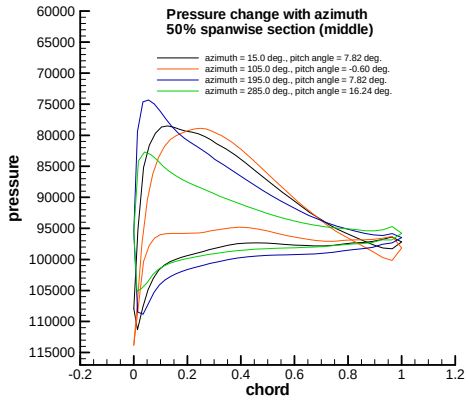

Figure 8c. Forward, 81.23 knots

Figure 8. Section pressure distributions at 50% blade span-wise location

	Blade1	Blade2	Blade3	Blade4
Case1	7.43	1.27	7.43	13.59
Case2	9.20	3.20	9.20	15.20
Case3	7.82	-0.60	7.82	16.24

Table 5. Pitch angles of the blades, degrees

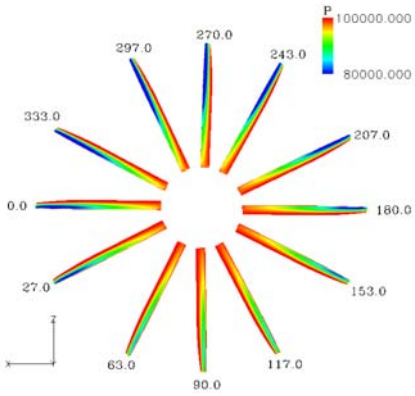

Figure 9a. Hover

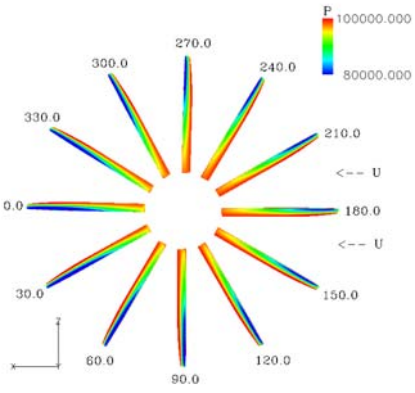

Figure 9b. Forward, 18.86 knots

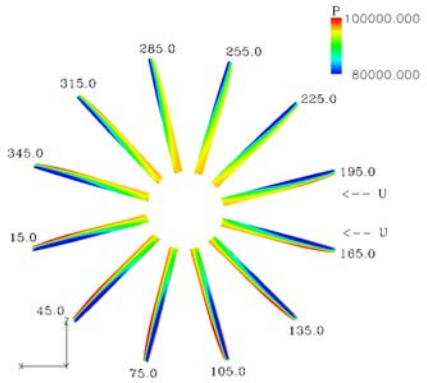

Figure 9c. Forward, 81.23 knots

Figure 9. Pressure distributions on a blade upper surface at various azimuth angles

The real-time flight measurements in reference 1 were taken at 256 scattered points on the surface of fuselage from the leading-edge nose region to the aft region of the vertical tail. The pressure data collected at these points were time-averaged as the rotor blades on top of the fuselage went through their cyclic motions. The time-averaged pressure data of the computation at 5 station cuts on the fuselage surface, as shown in Figures 10, were extracted out and compared with the measured data at the points fallen into or close to the corresponding station cuts. It is observed that the pressure change in different parts on the fuselage is much smaller compared with that on the blade surfaces. The comparisons are presented in Figures 11 through 15. Since the tail rotor, engine inlet and exhaust were not considered and only Euler solution was simulated in the present study (The viscosity and turbulence are dominant in some parts of such complex fuselage), these comparisons can only be considered as a qualitative check rather than the quantitative benchmark. On the fuselage (Figures 11, 12 and 13) and the stabilizers (Figures 14 and 15), the computed results agree well with the measurements. On the fuselage, asymmetry can be seen in these figures for hover and low forward speed conditions. For the hover case, the asymmetry is only from the unidirectional rotation of the rotor from starboard side to port side. For the low forward flight condition, the rotation of the rotor still impacts on the fuselage. The asymmetry is both from the unidirectional rotation of the rotor and the non-zero sideslip angle (11.93 degrees). For the high forward flight condition, as mentioned earlier, the air passing through the rotor system is nearly horizontal. The rotor has much less impact on the fuselage. Therefore, the pressure and other parameters have shown an almost symmetry for the flow case with a small sideslip angle (-1.39 degrees) on the symmetrical fuselage. These changes can also be observed in Figure 16. The more impact on the upper surface than the lower surface of the fuselage from the rotation of the rotor is expected.

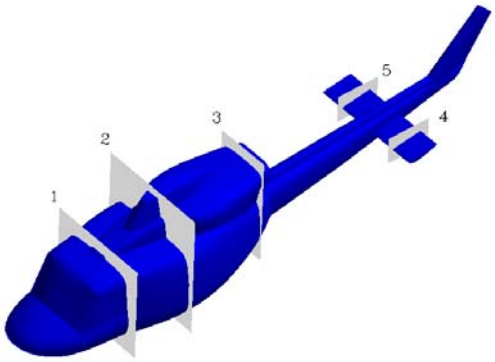

Figure 10. Station cuts on the fuselage

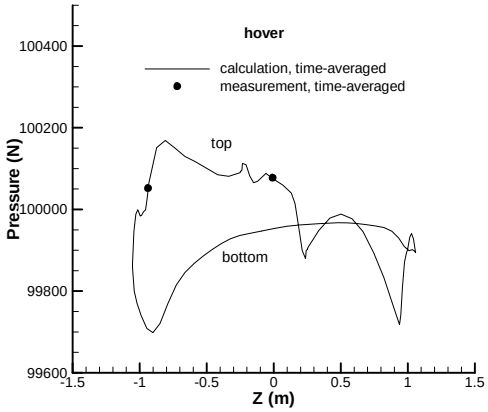

Figure 11a. Hover

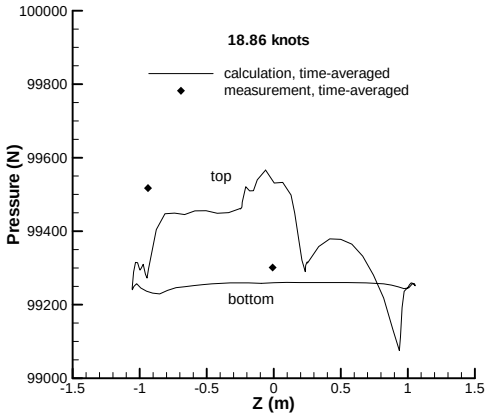

Figure 11b. Forward, 18.86 knots

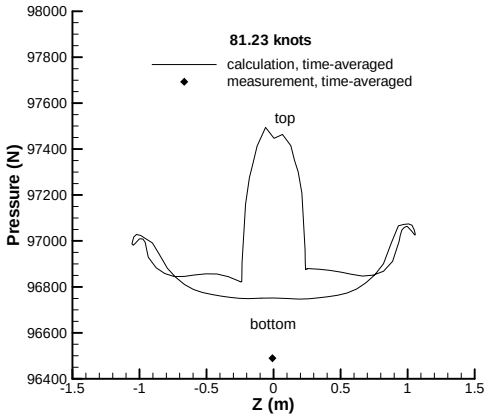

Figure 11c. Forward, 81.23 knots

Figure 11. Pressure distribution on the fuselage, X=1.72919m

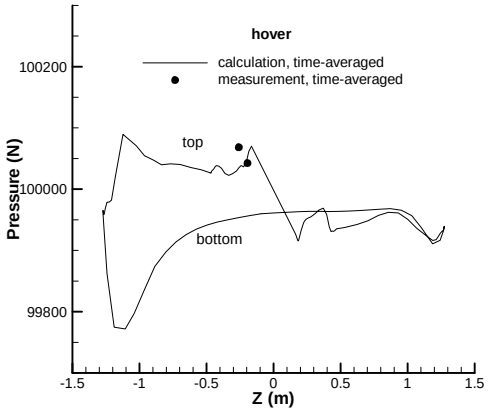

Figure 12a. Hover

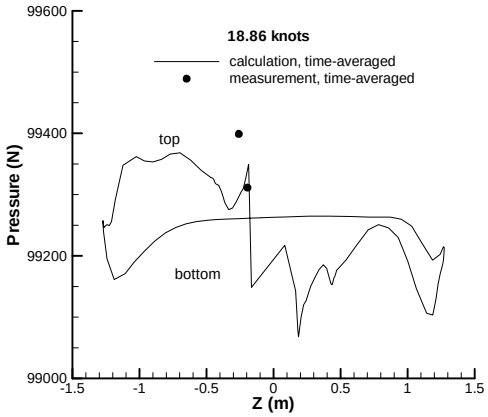

Figure 12b. Forward, 18.86 knots

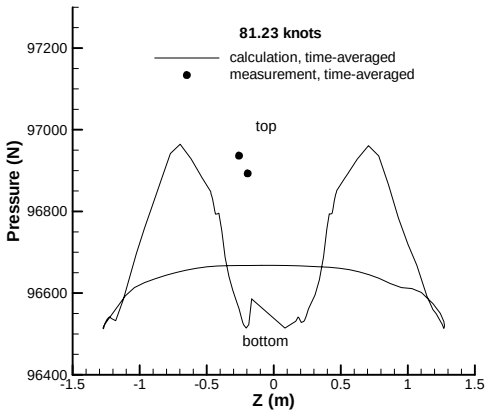

Figure 12c. Forward, 81.23 knots

Figure 12. Pressure distribution on the fuselage, X=3.17252m

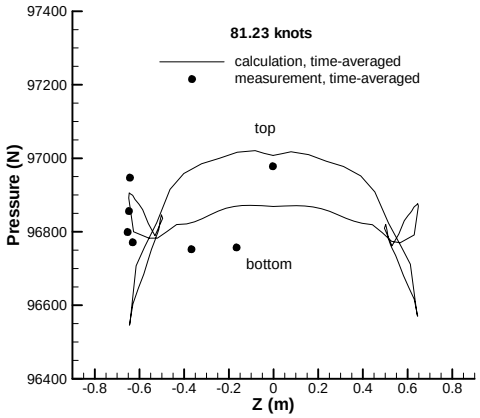

Figure 13c. Forward, 81.23 knots

Figure 13. Pressure distribution on the fuselage, X=5.61433m

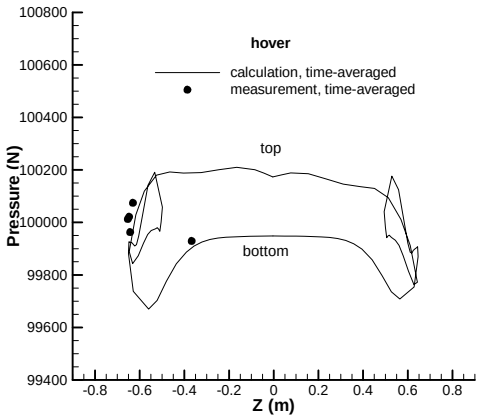

Figure 13a. Hover

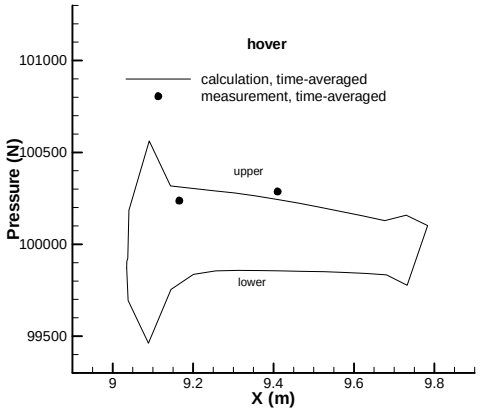

Figure 14a. Hover

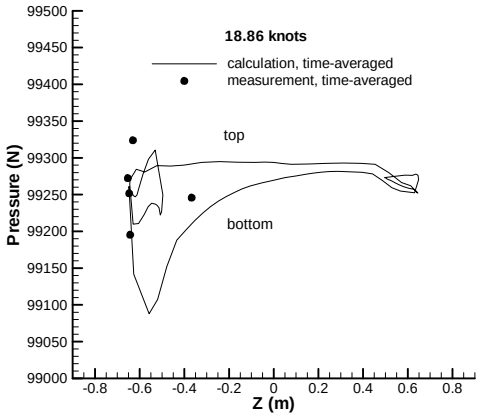

Figure 13b. Forward, 18.86 knots

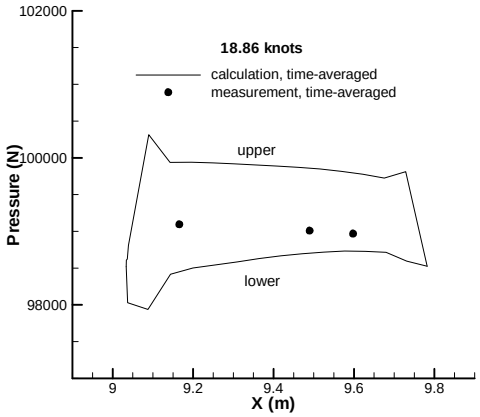

Figure 14b. Forward, 18.86 knots

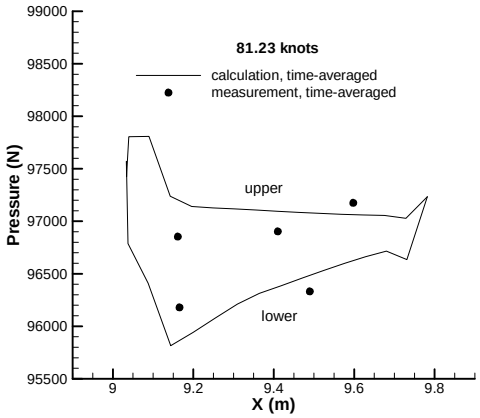

Figure 14c. Forward, 81.23 knots

Figure 14. Pressure distributions on the stabilizer section, port-stop side, middle section (Z=0.88m)

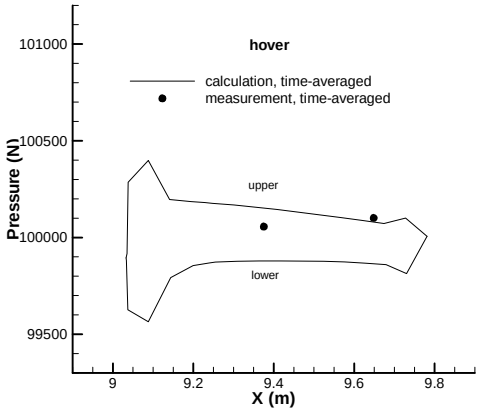

Figure 15a. Hover

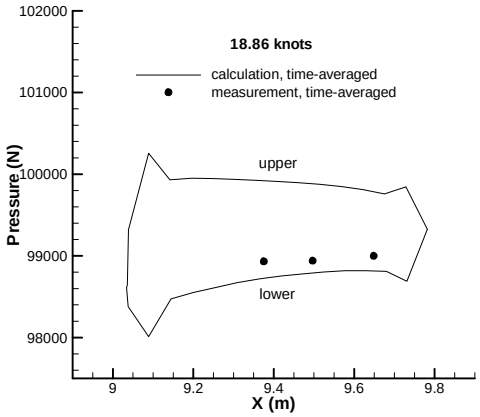

Figure 15b. Forward, 18.86 knots

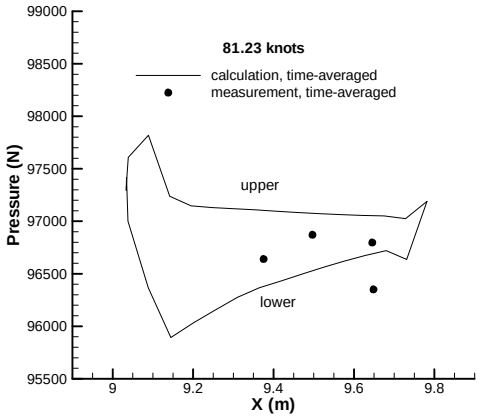

Figure 15c. Forward, 81.23 knots

Figure 15. Pressure distributions on the stabilizer section, starboard side, middle section (Z=-0.79m)

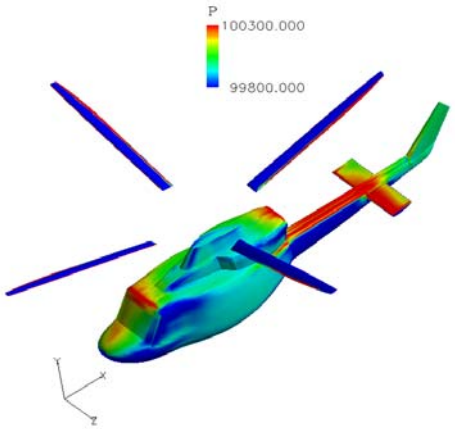

Figure 16a. Hover

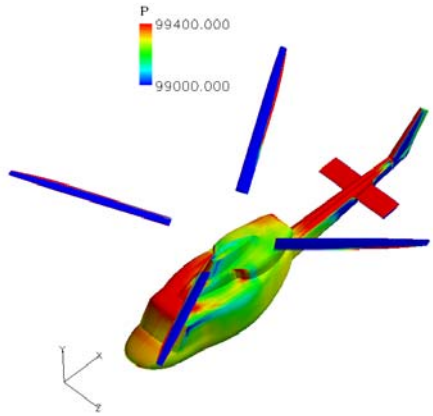

Figure 16b. Forward, 18.86 knots

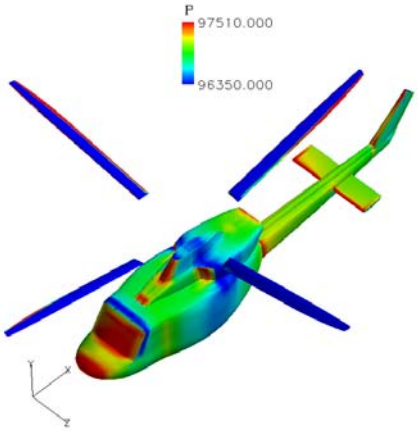

Figure 16c. Forward, 81.23 knots

Figure 16. Time-averaged pressure distributions

6. CONCLUSIONS

Numerical simulation was carried out to investigate the unsteady flow past a Bell 412 helicopter (fuselage and main rotor) in hover, low and high forward flight conditions with rotor blades moving in real-time. Collective and cyclic pitch change effects were also included using a Chimera moving grid method.

The pressure distributions on the rotor blades were reasonable. They are periodically changing with the pitch motion of the blades and the rotation of the rotor. The load difference between blades 1 and 3 with the same pitch angle showed the specific characteristic of unsteady flows. The flow also demonstrated the characteristic of retreating and advancing blades.

The calibrated relation between rotor-blade pitch angle and control positions was verified by the comparison of computational total lift against the measured helicopter weight in hover.

Pressure measurements on the fuselage qualitatively agreed with the computational results at discrete locations. With the increasing of the forward speed, the impact on the fuselage from the rotation of the rotor is less and less. The unidirectional rotation of the rotor leads to flow asymmetry on the fuselage for hover and low forward flight conditions.

It is recommended that the tail rotor, engine inlet and exhaust should be considered and Navier-Stokes solution should be computed for more accurate simulations. The same motion schedule should be used to investigate the translational lift and the aerodynamic improvement of the tail rotor with the increase of the forward speed.

The investigation and the comparison with flight data indicated that the CFD-FASTRAN flow solver is capable of capturing the unsteady aerodynamic features of rotor flows within a reasonable and acceptable accuracy.

ACKNOWLEDGMENTS

This work was carried out in collaboration with the Canadian Department of National Defense (DND). The authors would like to thank Warren Dool in the Design Office of IAR for his working on making the original CAD geometry usable for CFD and Dr. Jichao Su for his careful checking of the paper.

REFERENCES

1. B. E. Wake and F. D. Baeder, Evaluation of a Navier-Stokes Analysis Method for Hover Performance Prediction, Journal of the American Helicopter Society, Vol. 41, No. 1, January 1996.
2. P. Beaumier, K. Pahlke and E. Celli, Navier- Stokes Prediction of Helicopter Rotor Performance in Hover Including Aero-Elastic Effects, American Helicopter Society 56th Annual Forum, Virginia Beach, VA, May 2000.
3. H. Pomin and S. Wagner, Navier-Stokes Analysis of Helicopter Rotor Aerodynamics in Hover and Forward Flight, AIAA Paper 2001-0998, 39th Aerospace Sciences Meeting and Exhibit, Reno, NV, January 2001.
4. R. C. Strawn and M. J. Djomehri, Computational Modeling of Hovering Rotor and Wake Aerodynamics, American Helicopter Society 57th Annual Forum, Washington, DC, May 2001.
5. H. J. Kang, Unstructured Mesh Navier-Stokes Calculations of the Flow Field of a Helicopter Rotor in Hover, Journal of the American Helicopter Society, Vol. 47, No. 2, April 2002.
6. C. Benoit, Three-Dimensional Inviscid Isolated Rotor Calculations Using Chimera and Automatic Cartesian Partitioning Methods, Journal of the American Helicopter Society, Vol. 48, No. 2, April 2003.
7. Y. Park, Simulation of Unsteady Rotor Flow Field Using Unstructured Adaptive Sliding Meshes, Journal of the American Helicopter Society, Vol. 49, No. 4, October 2004.
8. H. Xu and S. Zhang, "Aerodynamic Investigations of Unsteady Flow past Robin Helicopter with Four-Bladed Rotor in Forward-Flight", 32nd European Rotorcraft Forum, September 11-14, 2006, Maastricht, The Netherlands.
9. F. Zhang, H. Xu, N. G. Ball and A.W. Gubbels, CFD Simulation of Fully Developed Unsteady Flow past a Bell 412 Helicopter in Hover, International Forum on Rotorcraft Multidisciplinary Technology, October 15-17, 2007, Seoul, South Korea.
10. CFD-FASTRAN user manuals, ESI Group, Paris, France.
11. A.W. Gubbels, S. Carignan, D. Ellis, J. Dillon, M. Bastian and C. Swail, NRC Bell 412 Aircraft Fuselage Pressure and Rotor State Data Collection Flight Test, Technical Report, Institute for Aerospace Research, National Research Council Canada, November 2005.